The final report on AOARD 05-4055

Quantum Functional Semiconductor Research Center
Dongguk University, Korea

March 29, 2006

Report Documentation Page

Form Approved
OMB No. 0704-0188

1. REPORT DATE	2. REPORT TYPE	3. DATES COVERED
26 JUL 2006	**Final Report (Technical)**	**29-03-2005 to 29-05-2006**

4. TITLE AND SUBTITLE	5a. CONTRACT NUMBER
Indium Gallium Nitride/Gallium Nitride (InGaN/GaN) Nanorod Superlattice (SL)	**FA520905P0366**
	5b. GRANT NUMBER
	5c. PROGRAM ELEMENT NUMBER
6. AUTHOR(S) **Tea Won Kang**	5d. PROJECT NUMBER
	5e. TASK NUMBER
	5f. WORK UNIT NUMBER
7. PERFORMING ORGANIZATION NAME(S) AND ADDRESS(ES) **Dongguk University,Pil-dong 3-26, Jung-gu,Seoul 100-715, Korea (South),NA,100715**	8. PERFORMING ORGANIZATION REPORT NUMBER **AOARD-054055**
9. SPONSORING/MONITORING AGENCY NAME(S) AND ADDRESS(ES) **The US Resarch Labolatory, AOARD/AFOSR, Unit 45002, APO, AP, 96337-5002**	10. SPONSOR/MONITOR'S ACRONYM(S) **AOARD/AFOSR**
	11. SPONSOR/MONITOR'S REPORT NUMBER(S) **AOARD-054055**

12. DISTRIBUTION/AVAILABILITY STATEMENT
Approved for public release; distribution unlimited

13. SUPPLEMENTARY NOTES

14. ABSTRACT

The growth condition, electrical, and optical properties of GaN nanorods grown on Si(111) substrates are investigated. The GaN nanorods were grown with a different growth time by using rf-plasma assisted molecular-beam epitaxy. It is clearly demonstrated that the critical diameter for defects-free GaN nanorods is determined to be below ~140 nm under the N-rich condition. Magnesium-doped GaN nanorods were also grown with the same growth condition. Two emission lines corresponding blue emission at about 3.26 and 3.18 eV were observed. These peaks are attributed to conduction band-to-shallow acceptor transitions and to defects associated with column/substrate interface-shallow Mg acceptor complexes, respectively. Finally, they have fabricated a p-n junction diode using the GaN nanorod. The GaN nanorod was patterned on SiO2 substrate by using E-beam lithography. The current-voltage curve exhibits strong temperature dependence, suggesting that thermionic emission over a barrier dominates. This barrier is most likely corresponding to emission from a deep level in the band. The deep level appears to be an electron trap at Ec-0.40 eV below the conduction band with a capture cross section of 2.22  10-16 cm2 near the depletion region of the p-n juction.

15. SUBJECT TERMS
Nanotechnology, Optoelectronics

16. SECURITY CLASSIFICATION OF:			17. LIMITATION OF ABSTRACT	18. NUMBER OF PAGES	19a. NAME OF RESPONSIBLE PERSON
a. REPORT	b. ABSTRACT	c. THIS PAGE			
unclassified	**unclassified**	**unclassified**		**19**	

Dear Dr. Mah
I have conducted the project supported by the AOARD fund. I really appreciate your concerning for the AOARD 05-4405 project. The research term of this project is March 29 2005 to March 28 2006. And I am now sending the final report on AOARD 05-4405. If you have any comment or question about this, just let me know. Thank you again for your supporting to AOARD project.

- Principal investigator: Prof. T. W. Kang
- Institution: Quantum functional Semiconductor Research Center (QSRC), Dongguk University
- Title of project: Indium Gallium Nitride/Gallium Nitride (InGaN/GaN) Nanorods Superlattice (SL)
- Research term: March 29 2005 ~ March 28 2006
- Ref: AOARD 05-4055
- Published or to be published results from our project

1. The recombination mechanism of Mg-doped GaN nanorods grown by plasma-assisted molecular-beam epitaxy. *Nanotechnology.* **17,** 913~916 (2006).
2. Optical properties of GaN nanorods grown by molecular-beam epitaxy; dependence on growth time. *Nanotechnology* **17,** 952~955 (2006).
3. Electron trap s level in GaN nanorod p-n junction grown by molecular-beam epitaxy . To be published to *Appl Phys. Lett.* (2006). Accepted with minor revision.
4. Enhancement of free-carrier screening due to tunneling in coupled asymmetric GaN/AlGaN quantum discs. To be published to *Appl Phys. Lett.* (2006). Accepted with minor revision

Indium Gallium Nitride/Gallium Nitride (InGaN/GaN) Nanorods Superlattice (SL)

Abstract

The growth condition, electrical, and optical properties of GaN nanorods grown on Si(111) substrates are investigated. The GaN nanorods were grown with a different growth time by using rf-plasma assisted molecular-beam epitaxy. It is clearly demonstrated that the critical diameter for defects-free GaN nanorods is determined to be below ~140 nm under the N-rich condition. Magnesium-doped GaN nanorods were also grown with the same growth condition. Two emission lines corresponding blue emission at about 3.26 and 3.18 eV were observed. These peaks are attributed to conduction band-to-shallow acceptor transitions and to defects associated with column/substrate interface-shallow Mg acceptor complexes, respectively. Finally, we have fabricated a *p-n* junction diode using the GaN nanorod. The GaN nanorod was patterned on SiO_2 substrate by using E-beam lithography. The current-voltage curve exhibits strong temperature dependence, suggesting that thermionic emission over a barrier dominates. This barrier is most likely corresponding to emission from a deep level in the band. The deep level appears to be an electron trap at Ec-0.40 eV below the conduction band with a capture cross section of 2.22×10^{-16} cm^2 near the depletion region of the *p-n* juction.

I. Introduction

One-dimensional (1D) structures (nanowires or nano-rods) of nanometer-scale gallium nitride (GaN) are known to have great prospects in fundamental physics and novel technological applications [1,2]. Because of the large band gap and structural confinements of the GaN nano-structure, for example, the fabrication of visible and UV optoelectronic devices with relatively low power consumption is potentially feasible[3,4]. These studies have mainly focused on zero-dimensional quantum dot and two-dimensional quantum well structures. However, one dimensional nanometer-scale GaN structures can provide a unique opportunity for understanding electronic, optical, and mechanical properties of the material. Recently, GaN work has been further extended to GaN-based nanotubes and nanowires [5-7]. It is reported that dislocation- and strain-free GaN materials can be obtained by forming nano-scale structures, such as columnar structures[8-10] and pyramidal hillocks[11] utilizing various methods, such as catalytic growth, patterning technique, and self-assembling process. GaN nanorod free from strain was reported by Seo *et al* [12]. For the past several years considerable effort has been made on the synthesis of 1D GaN structures: for example, through a carbon nanotube-confined reaction [13], template and catalytic synthesis [7], sublimation of GaN powder under a flowing ammonia atmosphere [14], and direct reaction of metal Ga vapour with flowing

ammonia [15]. In particular, recent development of self-assembled nanorods formed on silicon [16,17] and sapphire [16,18] substrates at an unprecedented pace is promising due to high quality of nanorods and relatively easy size controllability. In addition, the achievement of *p*-type doping of III-nitride semiconductors was an important step in the development of optoelectronic devices such as *p-n* junction diodes. Among the dopants, Magnesium (Mg) is widely used to make the *p*-type GaN because it exhibits the lowest activation energy of 0.16 eV [19]. A number of studies of Mg-doped GaN epilayers have been performed using photoluminescence spectroscopy, in which two photoluminescence bands are normally observed at 3.27-3.1 eV and at ~2.8 eV. Considering previous investigations, the former is attributed to the optical transition from the conduction band to the Mg acceptor level (e-A transition), zero-phonon donor-acceptor-pair (DAP) recombination [20-23] or shallow Mg impurities [24], and the latter is assigned to the transition from deep donors to a shallow Mg acceptors [20], and a Mg complex [21,25]. However, the origins of these transitions are still controversial. Moreover, in the case of *p*-GaN epilayers, these results are inferred from the unresolved luminescence peak lineshape, while in the case of nanorod the PL peak is well resolved due to the high crystal quality. Recently we reported on the optical properties of undoped GaN nanorods [26].

In this work, first, we report the growth and optical properties of GaN nanorods grown on Si (111) substrates by using rf plasma assisted molecular-beam epitaxy (PAMBE) as a function of growth time ranging from 5 min to 3 hours. Second, we report the recombination mechanism of Mg-doped GaN nanorods. We clearly observed the blue emission line at about 3.18 and 3.26 eV related to Mg-acceptors. The optical characterization of the transitions was undertaken by time-integrated (TI) and time-resolved photoluminescence (TR-PL) and the origins of the observed emission bands are discussed below. Finally, we present the electrical properties of nanorod p-n junction diode. In order to study the deep level defects in the p-n junction region, deep level transient spectroscopy (DLTS) measurements were carried out. Prior to measuring DLTS, temperature-dependent current-voltage (I-V) measurements were performed.

II. Experimental procedure

The samples used in this study were grown on Si (111) substrates without any buffer layer by using rf-PAMBE. The Si substrates were degreased and etched with HF. A reconstructed (7×7) reflection high energy electron diffraction (RHEED) pattern was obtained for the Si substrate after thermal treatment for 30 min at 1000 °C. After deoxidation, the substrate temperature was lowered down to 800 °C for growing. The substrate temperature was consistently monitored and controlled by infrared pyrometer. It must be noted that, unlike the previous reports, GaN layers were directly grown on Si substrates instead of forming a nucleation layer such as low temperature AlN buffer or metal catalytic growth prior to the GaN deposition. The growth time (t_g) has been varied from 5 min to 3 hours in order to investigate the early stage of nanorod formation. The Ga source is 7N5 pure metal in a conventional effusion cell. The nitrogen of 6N purity is further purified through a nitrogen purifier and then introduced into a plasma generator. Other growth parameters except t_g were fixed. All the growth conditions were N-rich. More detailed growth conditions can be found in ref. [27]. To achieve *n*- and *p*-GaN nanorods, solid Si and Mg were used as dopants, respectively. The carrier concentrations were evaluated to be 3×10^{18} cm^{-3} for the *n*-GaN nanorod and 1×10^{17} cm^{-3} for the *p*-GaN nanorod. The carrier concentrations were calibrated by a standard *n*- and *p*-GaN epilayers grown under the same temperature of the Si and Mg effusion cell.

In order to characterize the growth condition, electrical, and optical properties of the nanorods, high-resolution field emission scanning electron microscope (FESEM), PL, Catholuminescence (CL), and DLTS measurements were carried out. For TI-PL measurements, a commercial Renishaw 'RM-series' spectrometer/microscope system employing an external 325 nm Kimmon continuous wave (CW) He-Cd laser as an excitation source was used. TR-PL measurements were carried out using a frequency-tripled Ti-Sapphire laser operating at 266 nm and a commercial time correlated single photon counting (TC-SPC) system with a time resolution of 150 ps. In order to study the deep levels in the depletion region, we patterned linear electrodes of Ti/Au between the *p*- and *n*-GaN nanorod regions using E-beam lithography. The Ti/Au electrode showed Ohmic contact [28]. A rapid thermal annealing at 700 °C for 30 s was performed. During the DLTS measurement, an amplified transient signal was processed by electronic circuit, which consists of an A/D convertor and a microcomputer. To characterize any deep level defects, DLTS measurements were

performed at temperatures in the range 77 ~ 300 K, using a scanning temperature rate of 5 K/min. The height and filling width of the pulse were 1 V and 5 ms, respectively. DLTS spectra were taken at different rate windows from 4.33 to 69.31 sec^{-1}.

III. Results and discussion

FESEM images of self-assembled GaN vertical nanorods for various growth times are shown in Fig. 1. The epitaxial growth proceeds nominally just below stoichiometry (defined as a III/V ratio at which the growth rate saturates) [27]. As expected in the initial stage, N-rich conditions lead to columnar morphologies. These columnars are aligned along the (0001) direction. Similar columnar-GaN formed on silicon and sapphire substrates grown by MOCVD and MBE were also reported by other groups [29-31]. As the growth proceeds, compact columnar nanorods are grown with almost the same diameter and height. When the columnar base reaches close to ~ 400 nm, hexagonal nanorods start to protrude from the columnar base. The nanorods have a lateral dimension from 30 to 350 nm and height up to 3 μm with various densities, depending on growth parameters. As t_g is increased further, its average diameter and height increases. The insets of the Fig. 1 show top views of the nanorods.

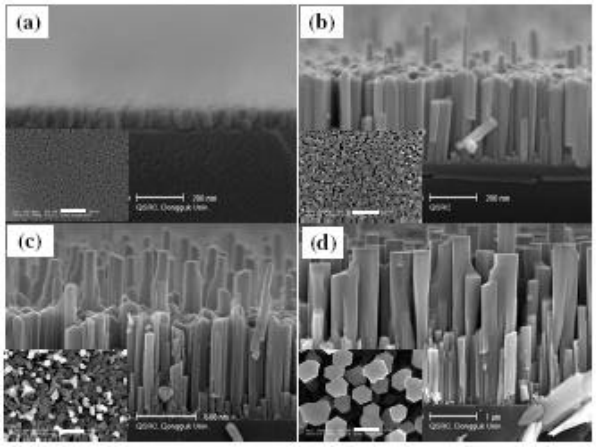

Fig. 1. FESEM micrographs of GaN nano-rods directly grown on Si (111) substrates for various t_g. (a) 5 min, (b) 20 min, (c) 1 hour, and (d) 3 hours. The insets of each figure present the plan-view images and all the scale bars are 500 nm

Figure 2 shows the t_g dependence of average nanorod diameter. The average diameter slowly increases at a growth rate of ~90 nm/h until ~90 min and at a growth rate of ~136 nm/h afterwards. This means that the growth rate of the lateral direction (nanorod diameter) becomes faster than that of the vertical direction (nanorod length), inducing defects such as points and threading dislocations. The insets present the density of nanorods as a function of t_g. The density of nanorods decreases with increasing t_g, resulting in the increase of nanorods' diameter. This is due to the coalescence of neighbouring nanorods. This could introduce the formation of threading dislocations (TDs) and other defects at the boundary. Similarly, it is well known that for GaN islands grown by MOVPE, their coalescence induce the generation of TDs at the lateral facets.

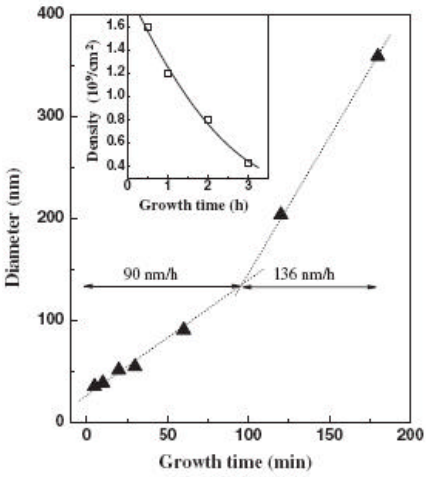

Fig. 2. Average diameter of the GaN nanorods as a function of t_g. The insets show the density of nanorod.

Figure 3(a) shows the low-temperature (10 K) PL spectra of the GaN nanorods for different t_g. Excitonic emission is clearly observed around 3.47 eV, which corresponds to a neutral donor bound exciton (D^0X). The higher energy shoulder composes of free-exciton (FX) emissions. The PL spectrum for the sample with t_g of 5 min shows a very broad and weak emission without noticeable features, probably due to the poor crystal quality. A clearer emission peak with a full width at half maximum (FWHM) of 165 meV is observed in the sample with t_g of 10 min. To accurately extract more detailed information such as peak positions and FWHM of these PL spectra, we reconstructed the spectra by using Gauss-Lorentzian line shape function and multi-peak analysis was performed. This broad emission peak consists of excitonic emission and donor-acceptor transition (DAP) related to defects in the compact region. With increasing t_g up to 30 min, three emission peaks are clearly resolved at 3.22, 3.33, and 3.47 eV. As mentioned above, the 3.47 eV emission corresponds to D^0X, and the others are probably due to defect levels in the band gap of the bottom GaN compact region. However, the 3.22 eV and 3.33 eV peaks disappear as t_g is further increased up to 1 hour. After t_g of ~ 90 min the length of the compact region almost saturates. On the other hand, the length of the nanorods linearly increases with increasing t_g. In addition, another defects-related peak (marked with arrows) is also observed near 3.41 eV for samples grown longer than 60 min, but this peak can not clearly seen for the samples grown shorter than 60 min because of its adjacent relatively large defect peak. Note that whilst the 3.41 eV peak is associated with the defects at the compact region/substrate interface, the 3.22 and 3.33 eV peaks are related with defects states in the compact region rather than at the interface. For the sample grown for 3 hours the intensity of excitonic emission rapidly decreases, and the emission near 3.3 eV is more clearly visible. In this case, the growth rate of the nanorod for the lateral (diameter) direction is higher than that of the vertical (length) direction. The high growth rate in the lateral direction leads to the high density of defects such as threading dislocation and point defects, decreasing the radiative recombination and increasing the non-radiative recombination.

Figure 3(b) summaries the PL peak position (E_p) and FWHM for the D^0X emission as a function of t_g. The peak continues to be blue-shifted up to t_g of 1 hour but turns to be red-shifted afterwards. This is due to the size effect of the GaN nanorods and is well consistent with the quantum confinement effect in the one-dimensional nanorods [31]. However, the measured FWHM shows opposite behaviors. The FWHM for the sample with t_g of ~80 min is estimated to be less than ~8 meV, which indicates the high quality of GaN nanorods. However, the FWHM decreases due to the statistical size fluctuation and effect of the compact region with increasing t_g up to ~80 min. Then, the FWHM rapidly increases with further increasing t_g, indicating a poor crystal quality. It is clear from the above argument that lateral growth of GaN nanorods is more dominant.

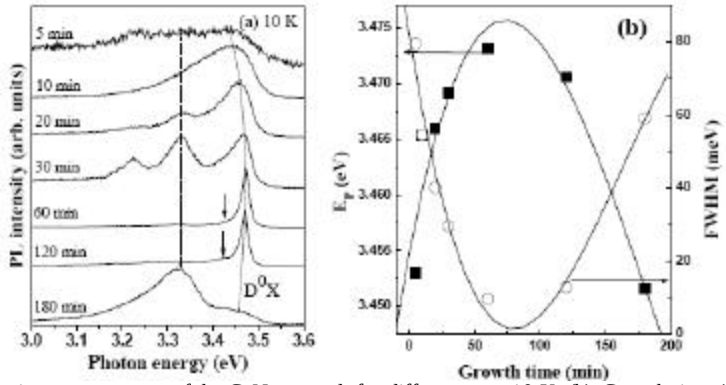

Fig. 3. (a) Photoluminescence spectra of the GaN nanorods for different t_g at 10 K. (b) Growth time (t_g) dependence of the peak position and full width at half maximum (FWHM) of the D^0X emission.

Figure 4 shows the temperature dependence of the D^0X peak position for GaN nanorods with t_g of 60min. It is well known that the temperature-dependent energy gap follows the Varshni's equation, $E_g(T) = E_g(0) - \alpha T^2/(\beta+T)$, where $E_g(T)$ is the transition energy at a given temperature T, $E_g(0)$ corresponds to the energy gap at 0 K. α and β are known as Varshni's thermal coefficient and Debye temperature, respectively [32]. The solid line in this figure is obtained by using least-square fitting. The fitted values are $\alpha = 5.3 \times 10^{-4}$ eV/K and $\beta = 487.5$ K. These values are in good agreement with our previous results [26] and also close to the reported ones for the D^0X transition [33]. To estimate corresponding activation energy of the D^0X process, we investigated the intensity variation of the peak as a function of temperature. The inset shows an Arrhenius plot of the peak's intensity. It is clear that the free exciton transition is thermally activated above 100 K. From the slope of the straight line the activation energy is estimated to be 27.9 meV, which is in good agreement with the exciton binding energy reported by Monemar [34] and Chichibu *et al* [35].

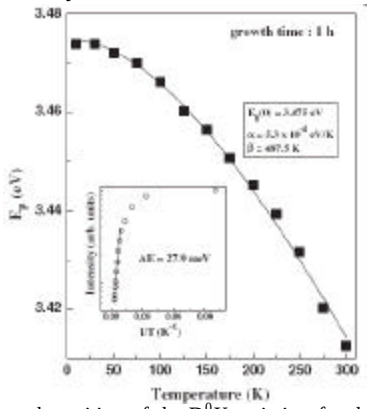

Fig. 4. Temperature-dependence of the peak position of the D^0X emission for the sample grown for 60 min. The solid line is a least-square fitted curve using the Varshni's equation (refer to the text for a detailed discussion). The inset shows an Arrhenius plot of the peak's intensity and thermal activation energy ΔE is estimated to be 27.9 meV.

Figure 5 shows TI-PL spectra as a function of temperature for Mg-doped GaN nanorods which have the growth time of 2 hours. Two dominant peaks near 3.18 and 3.26 eV are observed at 4.2 K. A neutral-acceptor-bound exciton (A^0X) line at about 3.46 eV is also observed. The intensities of the emission bands decrease gradually as the temperature increases. The intensity of the 3.26 eV emission line decreases more rapidly than that of the 3.18 eV emission line. Also we note that the behavior of the peak positions of the two

emission lines is different as the temperature increases. The energy of the 3.26 eV emission line redshifts with increasing temperature, whilst that of the 3.18 eV emission line does not change with temperature. This implies that the nature of two emission lines is different.

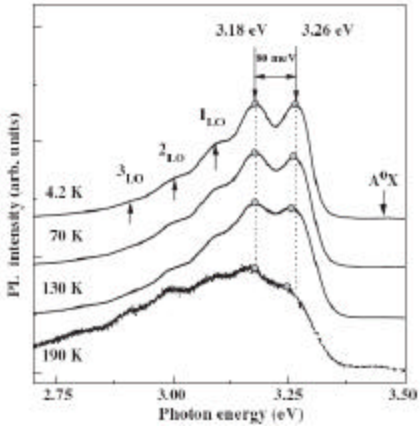

Fig. 5. Temperature-dependent time-integrated PL spectra from Mg-doped GaN nanorods.

It is most likely that the thermal characteristics of the 3.26 eV line arise from e-A transitions rather than from DAP transitions [24], because a blueshift with increasing temperature is expected in DAP transitions due to the enhancement of more closely spaced pairs [36]. Using the energy gap of GaN at low temperatures of 3.478 eV, we deduce that the Mg-related acceptor level is ~220 meV above the valence band, and this result agrees well with the reported values [36-39]. The shoulders seen in the emission below the 3.18 eV peak derive from LO phonon assisted recombination, related to the 3.18 eV line, given that the energy difference between the adjacent peaks is ~91 meV, which is consistent with the LO phonon energy in GaN. However, the energy difference of the two predominant peaks is ~80 meV, implying that the 3.18 eV emission line is not the first phonon replica of the 3.26 eV emission line.

Figure 6 shows the PL spectra of the sample as a function of excitation power taken at 4.2 K. The A^0X line is seen more clearly with increasing excitation power. The peak positions of A^0X are almost constant with increasing excitation power. In contrast to A^0X, the 3.26 eV and the 3.18 eV emission lines blueshift by 6 meV and 9.3 meV, respectively, as the excitation power is increased from 34.5 μW to 3.92 mW. In the case of the e-A transition, the blueshift can be explained by the increase of the quasi-Fermi level for the electrons in the conduction band and a sweep of the quasi-Fermi level for holes in the acceptor level (i.e. band filling effects) [22]. Since the number of acceptors should be limited because of the Mg concentration, the intensities of all the transitions are expected to be saturated at high excitation powers. The inset in Fig. 6 details the intensity dependence of these transitions in the GaN nanorods. This result indicates that the 3.26 and 3.18 eV lines are associated with the Mg acceptor level in the sample.

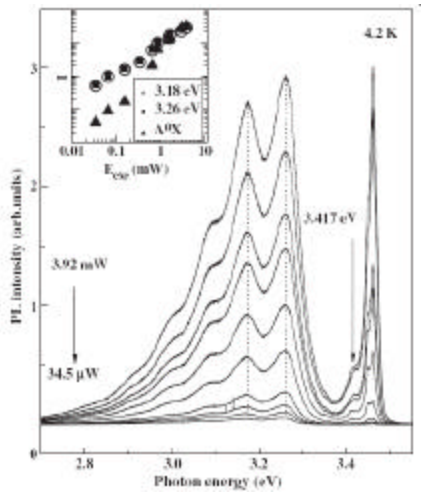

Fig. 6. Power-dependent PL spectra from Mg-doped GaN nanorods at 4.2 K. The inset shows the power-dependent PL intensities of the 3.26 (filled squares), 3.18 eV (empty circles), and A^0X (filled triangles) lines, respectively.

So far, we have concentrated on the 3.26 eV emission line. However, the origin of the 3.18 eV emission line is still ambiguous. Many suggestions have been proposed to explain the origin of this line. Firstly, we considered the reported deep level defects in GaN. Hacke *et al*. have found three Mg-related deep donor levels at 265, 400, and 615 meV by deep level transient spectroscopy [40]. Even if we consider other reported deep donor levels, observed by Lee and Hacke *et al.* [41,42], of 140 and 580 meV, the 3.18 eV line still does not correspond to expected values. Moreover, the PL properties of the 3.18 eV line described above do not match those expected of a DAP transition. Another possibility is that the 3.18 eV line is a new Mg-related acceptor level at ~300 meV above valence band. However, this assumption can not explain the lack of variation in the PL peak energy with temperature. In addition, TR-PL measurements indicate that the 3.26 and 3.18 eV emission lines are related to the same acceptor level, which will be discussed later.

In order to understand the origin of 3.18 eV line, we turn to the emission line at ~3.417 eV shown in Fig. 6. This PL peak is usually observed in compact or columnar GaN nanorods grown on Si(111). In a previous paper [26], we reported that this line originates from structural defects such as dislocations, present at the column/substrate interface. And this result agrees well with the values reported by Calleja *et al* [29]. The structural defects interact with local strain fields and/or electric fields associated with dislocations present at the interface at the base of the column. This structural defect may be distinguished from any ionized donor level formed by incorporation of impurities because the structural defects are barely affected by temperature. Similar structural defects are expected in our Mg-doped sample, giving rise to the line indicated at 3.417 eV in Fig. 6. We suggest that the defects make complexes with the Mg acceptor level. The local deformation potentials by dislocations may well localize carriers, and then localized carriers recombine with holes at the Mg-acceptor level. Thus, the localized carriers are not thermalized easily and should have long recombination lifetimes.

A schematic energy level diagram for the GaN:Mg nanorod system is presented in Fig. 7. As described earlier, the Mg acceptor level studied here is ~220 meV above the valence band. The structural defect level due to dislocations at the column/substrate interface is ~ 80 meV below the conduction band.

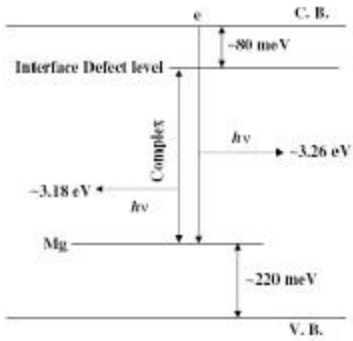

Fig. 7. A schematic level diagram for the recombination seen in the Mg-doped GaN nanorods.

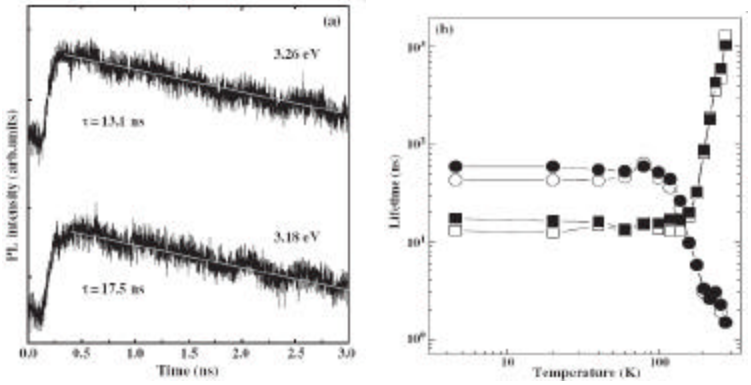

Fig. 8. (a) Time-resolved PL spectra recorded at 3.26 eV (upper line) and 3.18 eV (lower line) at 4.2 K. Both decay traces show single exponential decays with lifetimes of 13.1 and 17.5 ns, respectively. (b) A plot of radiative and nonradiative lifetime vs temperature for Mg-doped GaN nanorods. The filled and empty circles represent nonradiative lifetime for 3.18 and 3.26 eV line, respectively, and the filled and empty squares denote radiative lifetime for 3.18 and 3.26 eV line, respectively.

Further understanding of the origin of these emission lines can be obtained by studying their dynamical behavior using TR-PL spectroscopy. Figure 8(a) shows the TR-PL spectra of the 3.26 eV and 3.18 eV emission lines measured at 4.2 K. Given that the decay times are in the nanosecond range, this confirms once more that these emission bands are not DAP transitions, since DAP transitions have typical lifetimes of microseconds [44] and tend to exhibit non-exponential decays [43]. However, both the PL decay traces are single-exponential in character with decay times of 13.1 ns for the 3.26 eV line and 17.5 ns for the 3.18 eV line, respectively. The decay time of 13.1 ns for 3.26 eV line is comparable to that reported for e-A transitions in Mg-doped GaN in the literature [22]. And the 3.18 eV line shows a longer decay time, as expected. From the quantum efficiencies ($?=I_{pl}(T)/\ I_{pl}(4K)$) and effective decay times (t_{eff}) with temperature, radiative (t_r) and non-radiative lifetimes ($t_{\rm nr}$) can be deduced using the relations:

$$h = \frac{t_{eff}}{t_r},$$

$$\frac{1}{t_{eff}} = \frac{1}{t_r} + \frac{1}{t_{nr}}.$$

Fig. 8(b) shows the temperature dependence of the PL decay times at the above spectral peak positions. A decrease in PL efficiency and radiative lifetime is seen at temperatures above 120 K, and occurs simultaneously in both emission bands. This arises from an increased non-radiative recombination rate above

this temperature, and also supports the assertion that the two emission lines are associated with same acceptor level. This fact indicates that the quenching of the emission is due to thermal ionization of shallow neutral Mg acceptors as the temperature increases. In addition, we did not observe any deep level states that yield blue- and green-band emission, via e-A or DAP transitions, even at high temperatures [25,45]. This indicates that our sample does not have Mg-related deep levels, resulting in spectrally pure emission bands in comparison with other Mg-doped *p*-type GaN epilayers.

On the basis of above results, we have fabricated a *p-n* junction diode using the GaN nanorod. The spatial localization of the *p-n* junction diode was unambiguously determined by spatially-resolved monochromatic catholuminescence (CL) measurements. Figure 9(a) shows the CL spectrum of the nanorod *p-n* junction in the cross-sectional view measured at 300 K. A broad and strong peak near 3.39 eV is observed. Also a weak luminescence peak near 3.0 eV is observed. Fig. 9(b) shows the cross-sectional SEM image of the GaN nanorod with electron beam energy of 10 kV. Figs. 9(c) and (d) present the CL images at the same region shown in Fig. 9(b) taken at the emission energies of E_{CL} = 3.39 eV and E_{CL} = 3.00 V, respectively. The origin of the 3.39 and 3.00 eV emission energy comes from n-type GaN region doped with Si and p-type GaN region doped with Mg, respectively. These emission lines correspond to band edge transition (FX) and donor acceptor pair (DAP) transition, respectively. It is clear that the GaN nanorod *p-n* junction is well formed.

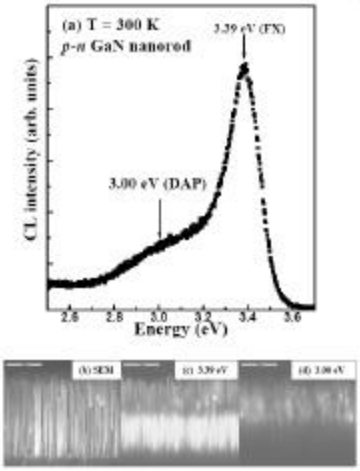

Fig. 9. Catholuminescence spectrum of the p-n junction GaN nanorod with an energy of 10 kV. (b) The cross-sectional view of high resolution scanning electron microscopy. Catholuminescence images at the same region shown in Fig. 9(b) taken at E_{CL} = 2.96 eV (c) and taken at E_{CL} = 3.00 eV (d). Scale bar is 2 μm.

The I-V characteristic curves of the *p-n* junction nanorod diode were measured at temperature range 6 to 300 K. Figure 10 shows the I-V curve measured at 6 K (closed square), 138 K (open circle), and 296 K (open triangle). The lower inset shows a FESEM image of the *p-n* junction GaN nanorod, which is attached to two Ti/Au electrodes. As shown in Fig. 10, the I-V characteristic curve shows nonlinear and clear rectifying behavior at 6 K with a turn on voltage of ~7.2 V for the forward bias and reverse bias break down of ~ -9 V. By increasing the temperature up to 296 K, the turn on voltage reduces to ~0.4 V and ~ -0.8 V for the forward and reverse bias, respectively. The I-V curve exhibits strong temperature dependence, suggesting that thermionic emission over a barrier dominates. This barrier is most likely corresponding to emission from a deep trap level to the band. Significant reverse bias leakage is observed in this nanorod diode, indicating the presence of trap levels within the band gap. These levels could be the defects associated with the side wall damage [46]. In our study, however, the side wall and threading dislocation effects are excluded because no distinct dislocation network and side wall damage are observed as shown in the upper inset of Fig. 10 which indicates an image of transmission electron microscopy (TEM) for the GaN nanorod. Unlike the results of

Cheng *et al* [47] the side view of nanorod show clear wall. Therefore, it is thought to be due to a defect of the nanorod.

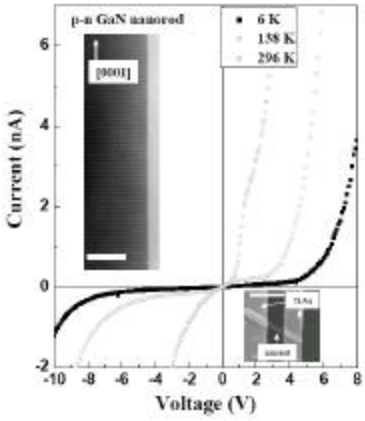

Fig. 10. The temperature-dependent I-V characteristic curve of the *p-n* junction GaN nanorod diode. The temperatures were 6 K (closed square), 138 K (open circle), and 296 K (open triangle) from the above curve. The lower inset shows the SEM image of the sample used in this study. Scale bar is 1 μm. The higher inset presents the TEM image of the GaN nanorod.

A study of deep levels is needed to determine which nature dominates. Figure 11 presents the DLTS spectrum with rate windows of 11.17 sec^{-1} for the GaN nanorod *p-n* junction diode. A DLTS signal was clearly observed near ~240 K. To extract more detailed information from the DLTS signals, the activation energy (E_T) and capture cross section (σ_T) were obtained from Arrhenius plot, which was plotted from DLTS signals at different rate windows. The inset of Fig. 11 presents the Arrhenius plots as a function of $Ln(e_nT^{-2})$ versus $1000/T_m$. The activation energy E_T was calculated to be 0.40 eV. To our knowledge there are no reports, with such a value for a deep level at the *p-n* junction region. Recent research has shown that a deep level electron trap at Ec-0.59 eV is formed on Si-implanted GaN n^+-*p* junction diode [48]. Asghar *et al* reported that the three deep levels, E1 (Ec-0.59), E2 (Ec-0.76), and E3 (Ec-0.96), exist in GaN *p-n* diode grown by metal-organic chemical vapor deposition [49]. The 0.58-0.62 eV level can be correlated with residual Mg impurities in the *n* side of the epitaxially grown p^+-*n* junction diode [50]. Hacke *et al* reported three Mg-related deep donor levels at 0.26, 0.40, and 0.62 eV by DLTS [51]. In many reports the activation energy is above ~0.59 eV. However, our result is not in agreement with reported values. The capture cross section σ_T is determined to be 2.22×10^{-16} cm^2. Although E_T is in good agreement with the reported values for Mg-related deep donor level, the σ_T value is quite different from the reported results [51,52]. Moreover, the hole traps with energy levels at 0.41, 0.49, and 0.59 eV above the valence band have been reported only on *p*-GaN epi-films [52,53]. And, normalized DLTS intensity of the nanorod, $\Delta C/C_0$, is 5 times lower than that of *p*-GaN epilayer. The estimated trap concentration of GaN nanorod is about 3×10^{14} cm^{-3} and 5 times lower, if they have the same doping density (N_A) with GaN epilayer.

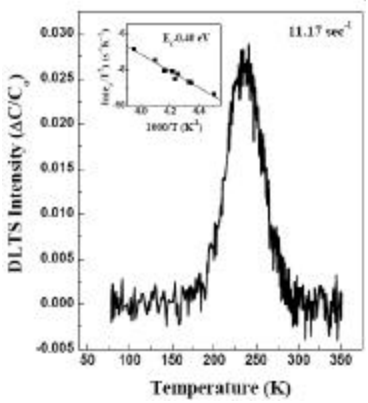

Fig. 11. The deep level transient spectroscopy signal of the GaN nanorod *p-n* junction diode measured at an emission rate window of 11.17 sec^{-1}. Inset shows the Arrhenius plots of the electron emission rate.

IV. Conclusions

We have investigated the growth and optical properties of dislocation-free vertical GaN nanorods grown on Si(111) substrates by rf-plasma assisted molecular-beam epitaxy, as a function of growth time. It is found that the average diameter of nanorods increases at a growth rate of ~90 nm/h until ~90 min but at a growth rate of ~136 nm/h afterwards. The optical properties of the nanorods are quickly degraded at the high growth rate in the lateral direction (nanorod diameter) in which defects are easily induced. The critical diameter of defects-free GaN nanorods is estimated to be below ~140 nm under the N-rich condition. In order to fabricate the *p-n* junction diode of GaN nanorod, we have also characterized optical transitions in Mg-doped GaN nanorod. A shallow Mg acceptor level was identified at ~220 meV above the valence band edge. Two emission lines related to Mg at about 3.26 and 3.18 eV are assigned to a conduction band to shallow acceptor (or e-A) transitions, and structural defect-related Mg complexes, respectively. Finally, we investigated the electrical properties of *p-n* junction diode. To measure DLTS, we patterned the GaN nanorod *p-n* junction diode by using E-beam lithography. The I-V characteristic curve shows nonlinear and clear rectifying behavior at 6 K with a turn on voltage of ~7.2 V for the forward bias and reverse bias break down of ~ -9 V. The deep defect level appears to be an electron trap at Ec-0.40 eV below the conduction band with a capture cross section of 2.22×10^{-16} cm^2 and the trap concentration is 5 times lower than that of the GaN epilayer. These defects-free GaN nano-structures may find many important applications in the future development of optical nano-devices based on nitride materials.

References

[1] F. A. Ponce and D. P. Bour, Nature **386,** 251 (1997).
[2] H. Morkoc and S. N. Mohammand, Science **267,** 51 (1995).
[3] C. M. Lieber, Solid State Commun. **107,** 607 (1998).
[4] S. Nakamura, T. Mukai, and M. Senoh, Appl. Phys. Lett. **64,** 1687 (1994).
[5] B. Xu, A. J. Lu, B. C. Pan, and Q. X. Yu, Phys. Rev. B **71,** 125434 (2005).
[6] J. Goldberger, R. He, Y. Zhang, S. Lee, H. Yan, H.-J. Choi, and P. Yang, Nature **422,** 599(2003).
[7] X. F. Duan and C. M. Lieber, J. Am. Chem. Soc. **122,** 188(2000).
[8] M. Yoshizawa, A. Kikuchi, N. Fujita, K. Kushi, H. Sasamoto, and K. Kishino, J. Cryst. Growth **189/190**, 138 (1998).
[9] I. M. Tiginyanu, V. V. Ursaki, V. V. Zalamai, S. Langa, S Hubbard, D. Pavlidis, and, H. Foll, Appl. Phys. Lett. **83,** 1551 (2003).
[10] T. Araki, Y. Chiba, M. Nobata, Y. Nishioka, and Y. Nanishi, J. Cryst. Growth **209,** 368 (2000).
[11] L. T. Romano and T. H. Myers, Appl. Phys. Lett. **71,** 3486 (1997).
[12] H. W. Seo, Q. Y. Chen, M. N. Iliev, W. K. Chu, L. W. Tu, C. L. Hsiao, and J. K. Meen, http://arxiv.org/abs/cond-mat/0503195
[13] W. Han, S. Fan, Q. Li, and Hu, Science **277,** 1287 (1997).
[14] Y. Li, X. L. Chen, Z. Y. Qiao, Y. G. Cao, and Y. C. Lan, J. Crystal Growth **213,** 408 (2000).
[15] M. He, I. Minus, P. Zhou, S. N. Mohammed, J. B. Halpern, R. Jacobs, W. L. Sarney, L. Salamanca-Riba, and R. D. Vispute, Appl. Phys. Lett. **77,** 3731 (2000).
[16] E. Calleja, M. A. Sanchez-Garcia, F. Calle, F. B. Naranjo, E. Munoz, U. Jahn, K. Ploog, J. Sanchez, J. M. Calleja, K. Saarinen, and P. Hautojarvi, Materials Science and Engineering B **82,** 2 (2001).
[17] J. Ristic, E. Calleja, M. A. Sanchez-Garcia, J. M. Ulloa, J. Sanchez-Paramo, J. M. Calleja, U. Jahn, A. Trampert, and K. H. Ploog, Phys. Rev. B **68,** 125305 (2003).
[18] M. Yoshizawa, A. Kikuchi, N. Fujita, K. Kushi, H. Sasamoto, and K. Kishino, J. Crystal Growth **189/190,** 138 (1998).
[19] I. Kasaki, H. Amano, M. Kito, and K. Hiramatsu, J. Lumin. **48-49,** 666 (1991).
[20] A. K. Viswanath, E. J. Shin, J. I. Lee, S. Yu, D. Kim, B. Kim, Y. Choi, and C. H. Hong, J. Appl. Phys. **83,** 2272 (1998).
[21] M. Llegems and R. Dingle, J. Appl. Phys. **44,** 4234 (1973).
[22] M. Smith, G. D. Chen, J. Y. Lin, H. X. Jiang, A. Salvador, B. N. Sverdlov, A. Botchkarev, H. Morkoc, and B. Goldberg, Appl. Phys. Lett. **68,** 1883 (1996).
[23] M. Ilegems and R. Dingle, J. Appl. Phys. **44,** 4234 (1973).
[24] J. M. Myoung, K. H. Shim, C. Kim, O. Gluschenkov, K. Kim, S. Kim, D. A. Turnbull, and S. G. Bishop, Appl. Phys. Lett. **69,** 2722 (1996).
[25] Y. Koide, Jr D E W, B. D. White, L. J. Brillson, M. Murakami, S. Kamiyama, H. Amano, and I. Akasaki, J. Appl. Phys. **92,** 3657 (2002).
[26] Y. S. Park, C. M. Park, D. J. Fu, T. W. Kang, and J. E. Oh, *Appl. Phys. Lett.* **85,** 5718 (2004).
[27] Y. S. Park, S. H. Lee, J. E. Oh, and T. W. Kang, J. Crystal Growth **282**, 313 (2005).
[28] J.-R. Kim, B.-K. Kim, I. J. Lee, J.-J. Kim, J. Kim, S. C. Lyu, and C. J. Lee, Phys. Rev. B **69**, 233303 (2004).
[29] E. Calleja, M. A. Sanchez-Garcia, F. J. Sanchez, F. Calle, F. B. Naranjo, E. Munoz, U. Jahn, and K. Ploog, Phys. Rev. B **62,** 16826 (2000).
[30] L. W. Tu, C. L. Hsiao, T. W. Chi, I. Lo, and K. Y. Hsieh, Appl. Phys. Lett. **82,** 1601 (2003).
[31] X. Duan, J. Wang, and C. M. Lieber, Appl. Phys. Lett. **76,** 1116 (2000).
[32] Y. P. Varshni, Physica **34,** 149 (1967).
[33] A. K. Viswanath, J. I. Lee, S. Yu, D. Kim, Y. Choi, and C.-H. Hong, J. Appl. Phys. **84,** 3848 (1998).
[34] B. Monemar, Phys. Rev. B **10,** 676 (1974).
[35] S. Chichibu, T. Azuhata, T. Sota, and S. Nakamura, J. Appl. Phys. **79**, 2784 (1996).
[36] O. Lagerstedt and B. Monemar, J. Appl. Phys. **45,** 2266 (1974).

[37] T. S. Jeong, C. J. Youn, M. S. Han, J. W. Yang, and K. Y. Lim, J. Cryst. Growth **259,** 267 (2003).
[38] L. Eckey, U. von Gfug, J. Holst, A. Hoffmann, A. Kaschner, H. Siegle, C. Thomsen, B. Schineller, K. Heime, M. Heuken, O. Schon, and Beccard, J. Appl. Phys. **84,** 5828 (1998).
[39] S. G. Bishop, *Gallium Arsenide Technolgy*, edited by D. K. Ferry (Howard W. Sams, Indiana, 1989), Vol. II, Chap. 11.
[40] P. Hacke, H. Nakayama, T. Detchprohm, K. Hiramatsu, and N. Sawaki, Appl. Phys. Lett. **68,** 1362 (1996).
[41] P. Hacke, T. Detchprohm, K. Hiramatsu, N. Sawaki, K. Tadatomo, and K. Miyake, J. Appl. Phys. **76,** 304 (1994).
[42] W. I. Lee, T. C. Huang, J. Guo, and M. S. Feng, Appl. Phys. Lett. **67,** 1721 (1995).
[43] D. G. Thomas, J. J. Hopfield, and W. M. Augustyniak, Phys. Rev. **140,** A202 (1965).
[44] R. Dingle, and M. Ilegems, Solid State Commun. **9**, 175 (1971).
[45] M. A. Reschikov, G.-C. Yi, and B. W. Wessels, Phys. Rev. B **59,** 13176 (1999).
[46] P. Kozodoy, J. P. Ibbetson, H. Marchand, P. T. Fini, S. Keller, J. S. Speck, S. P. DenBaars, and U. K. Mikshra, Appl. Phys. Lett. **73**, 975 (1998).
[47] G. Cheng, A. Kolmakov, Y. Zhang, M. Moskovits, R. Munden, M. Reed, G. Wang, D. Moses, and J. Zhang, Appl. Phys. Lett. **83**, 1578 (2003).
[48] X. D. Chen, Y. Huang, S. Fung, C. D. Beling, C. C. Ling, J. K. Sheu, M. L. Lee, G. C. Chi, and S. J. Chang, Appl. Phys. Lett. **82**, 3671 (2003).
[49] M. Asghar, P. Muret, B. Beaumont, and P. Gibart, Mater. Sci. and Eng. B **113**, 248 (2004).
[50] A. Hierro, D. Kwon, S. A. Ringel, M. Hansen, J. S. Speck, U. K. Mishra, and S. P. DenBaars, Appl. Phys. Lett. **76**, 3064 (2000).
[51] P. Hacke, H. Nakayama, T. Detchprohm, K. Hiramatsu, and N. Sawaki, Appl. Phys. Lett. **68**, 1362 (1996).
[52] H. Nagai, Q. S. Zhu, Y. Yawaguchi, K. Hiramatsu, and N. Sawaki, Appl. Phys. Lett. **73**, 2024 (1998).
[53] W. Gotz, N. M. Johson, and D. P. Bour, Appl. Phys. Lett. **68**, 3470 (1996).